Optics & Laser Technology 60 (2014) 116–123

Contents lists available at ScienceDirect

Optics & Laser Technology

journal homepage: www.elsevier.com/locate/optlastec

Fiber coupling efficiency analysis of free space optical communication systems with holographic modal wave-front sensor

Wei Liu [a], Wenxiao Shi [a,*], Kainan Yao [b,c], Jingtai Cao [a,b], Pengxia Wu [a], Xuefen Chi [a]

[a] College of Communication Engineering, Jilin University, 5372 Nanhu Road, Changchun 130012, China
[b] Changchun Institute of Optics, Fine Mechanics and Physics, Chinese Academy of Sciences, 3888 Nanhu Road, Changchun 130033, China
[c] Graduate School of Chinese Academy of Sciences, Beijing 100039, China

ARTICLE INFO

Article history:
Received 20 October 2013
Received in revised form
30 December 2013
Accepted 19 January 2014
Available online 8 February 2014

Keywords:
FSO communication
Holographic modal wave-front sensor
Fiber coupling efficiency

ABSTRACT

Degradation of fiber coupling efficiency, caused by atmospheric turbulence, seriously hinders the performance of free space optical (FSO) communication systems. Holographic modal wave-front sensor (HMWFS), noted for its fast detecting rates and insensitivity to beam scintillation, is creatively applied to FSO communication systems in this paper. We analyze the principle of HMWFS and the relationship between fiber coupling efficiency and Strehl rate in theory, then simulate wave-front aberrations detection and correction in FSO communication systems. Additionally, the impact on fiber coupling efficiency of the FSO communication systems before and after aberrations correction based on HMWFS is fully discussed. The results show that HMWFS cater for weak atmospheric turbulence with the root-mean-square (RMS) value of residual aberrations less than 0.04λ and the peak-to-valley (PV) value less than 0.25λ, while the fiber coupling efficiency is increased from nearly 30% to more than 70%.

1. Introduction

FSO communication systems transmit laser beam signals through the atmosphere, whose advantages include relatively low-cost, highly secure with dense spatial reuse, and low power usage per transmitted bit capabilities [1–3]. However, the atmospheric turbulence can have a tremendous impact on FSO communication systems [4–8], resulting in both phase and amplitude fluctuations of the received signal. Therefore, fiber coupling efficiency of the FSO communication system severely decreases and so does the system's performance.

Similar researches have been done before. Yamac [9] has deduced the relationship between the atmosphere refraction constant and the fiber coupling efficiency. Jing Ma [10] has analyzed the fiber coupling efficiency with the change of characteristic parameters of the localized distortion. Morio Toyoshima [11] has discussed the random angular jitter in relation to fiber coupling efficiency, and then analyzed the impact on bit error ratio.

Adaptive optics (AO) system can be applied to FSO communication systems to improve fiber coupling efficiency, by reducing the effects of atmospheric turbulence with wave-front aberrations correction [12–15]. The wave-front sensor (WFS) is a key component to detect spatiotemporally varying wave-front errors in AO system. Generally, the Shack–Hartmann wave-front sensor (SH-WFS) is widely used as an effective WFS [16–18]. However, considering the scintillation of the laser caused by atmospheric turbulence is so strong that SH-WFS might not be able to detect the laser intensity all the time. Sensor-less wave-front measurement technology has been developing rapidly. For instance, stochastic parallel gradient descent (SPGD) algorithm is proposed to control the wave-front correctors in AO systems, but the control bandwidth is not large enough and the control process may be divergent in a particular situation [19–23]. The algorithm based on a transport of an intensity equation-based numerical method is used to obtain the wave-front aberrations. The intensity and phase are both reconstructed by numerical computation, such as fast Fourier transform (FFT), and multi-grid. However, the algorithm is more complicated [24].

Recently, a new model wave-front sensor using the holographic phase or binary phase mark to measure directly the Zernike components of an aberrated wave-front was proposed [25,26]. The development of holography [27–29] provides a new thought for the model wave-front. A holographic modal wave-front sensor (HMWFS) provides an alternative method to detect the wave-front aberrations. HMWFS converts the phase information into intensity information, thus the phase information can be extracted from the relative intensity of pairs of focal spots [30–32]. The relative intensity information can be obtained by fast photo detectors and some simple circuits, for example the high-speed charge coupled device (CCD) camera, the Avalanche photon diode (APD) array and so on, so resulting in fast detecting rates. In this paper, we propose the method of wave-front detection based on HMWFS in FSO communication system, and analyze the impact on fiber coupling efficiency.

The remainder of this paper is organized as follows. Section 2 illustrates the principle and model of the holographic modal

* Corresponding author.
E-mail address: swx@jlu.edu.cn (W. Shi).

0030-3992/$ - see front matter © 2014 Elsevier Ltd. All rights reserved.
http://dx.doi.org/10.1016/j.optlastec.2014.01.013

wave-front sensing, HMWFS and the fiber coupling efficiency of FSO communication system. In Section 3, we simulate the procedure of wave-front aberrations detection based on HMWFS in the FSO communication systems, and discuss the impact on fiber coupling efficiency of the FSO communication systems before and after the aberrations correction based on HMWFS. In Section 4, we summarize and present our conclusions.

2. Theoretical analysis

2.1. Holographic modal wave-front sensing principle

We propose a FSO system wave-front sensing method based on HMWFS. The fundamental principle of holographic mode wave-front sensing is shown in Fig. 1.

Where the output laser beam is collimated into the standard plane wave after spatial filter P1, followed by a tunable aperture P2 matching the beam diameter to the clear aperture of a holograph.

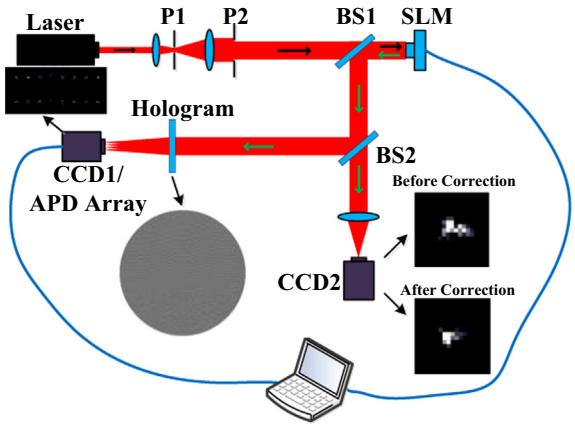

Fig. 1. Schematic view of the holographic modal wave-front sensing.

Through spatial light modulator (SLM) and beam splitter (BS1 and BS2), the plane wave, loaded with a measurable wave-front aberration, is split into two parts. One projects the before-correction laser image on CCD2, while the other entering holographic wave-front sensor forms multiple groups of spots on the focal plane of CCD1/APD array. By comparing the relative intensity of spots, the wave-front aberrations are obtained. Naturally, the corrected laser image can be obtained on CCD1/APD array by manipulating the SLM to correct wave-front aberrations.

2.2. Holographic modal wave-front sensor

The theoretical layout of HMWFS is shown in Fig. 2.

A hologram is recorded between an object beam with the minimum expected amplitude of the aberration $A_{\min}Z_i$ and a reference beam focused at point A on a distant detector, as shown in Fig. 2(a). Where Z_i is a Zernike polynomial of order i. $A_{\min}$ is the minimum measurable amplitude aberrations. The second hologram is then recorded between an object beam with the maximum amplitude of the aberration $A_{\max}Z_i$ and a reference beam focused at a different point B, as shown in Fig. 2(b). Where $A_{\max}$ is the maximum measurable amplitude aberration. According to the characteristics of the multiple holographic elements, a multiplexed hologram is generated by the pair of hologram [32].

When this hologram is reconstructed with an input beam with some amplitude, A_i, which is between the maximum and minimum values, there will be two focused beams produced at point A and point B, as shown in Fig. 2(c). The relative intensity of point A and point B is related to the coefficient of Zernike item. Thus, after a calibration, it is possible to obtain the amplitude simply by sensing the spot intensities.

Additionally, to increase the number of aberration detected modes, the multiplexed hologram needs only to be encoded with more pairs of holograms. Since the pairs of spots are spatial separate, the amplitudes of pairs of spots can be parallel read out through sensor array. Thus, the Zernike modal amplitude can

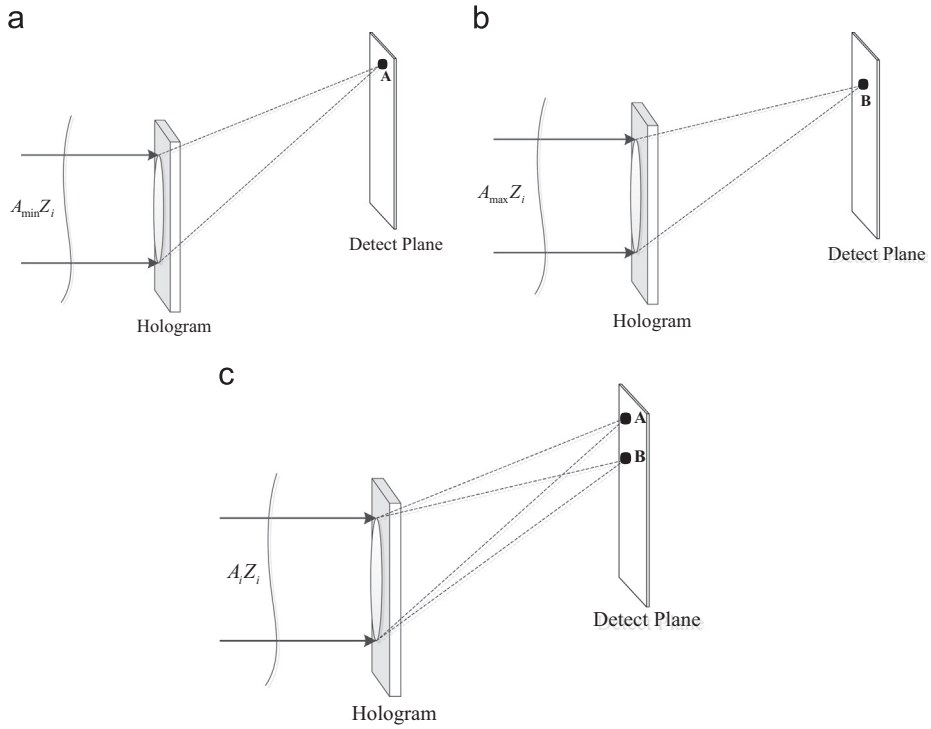

Fig. 2. The theory of HMWFS.

be obtained by comparing the relative intensity of pairs of spots, and then the wave-front aberrations are obtained.

In the mth hologram, another interfered beam is an aberration biased, the complex amplitude $U_{s,m}(r)$ is given by the following equation:

$$U_{S,m}(r_{S,m}) = U_{S,m,0}\exp[iW(r_{S,m})] \tag{1}$$

where $U_{S,m,0}$ is the amplitude of the interfered beam, $W(r_{S,m})$ is the phase of the interfered beam. Expand the phase item by orthogonal Zernike polynomial, as given by

$$W(r_{S,m}) = \sum_j \varepsilon_{m,j} Z_j \tag{2}$$

where $\varepsilon_{m,j}$ is the amplitude of the Zernike mode, Z_j is the Zernike polynomial of order j. In the following analysis, we assume that the multiplicity of the hologram is neglected. According to Fourier optics, suppose the amplitude of the signal laser beam is $U_{S,0}$, the phase function is $\phi(r_s)$, then the complex amplitude of the signal laser beam $U_S(r)$ can be expressed as

$$U_S(r) = U_{S,0}\exp[i\phi(r_s)] \tag{3}$$

Similarly, the complex amplitude of the reference laser beam $U_R(r)$ can be expressed as

$$U_R(r) = U_{R,0}\exp[i\phi(r_R)] \tag{4}$$

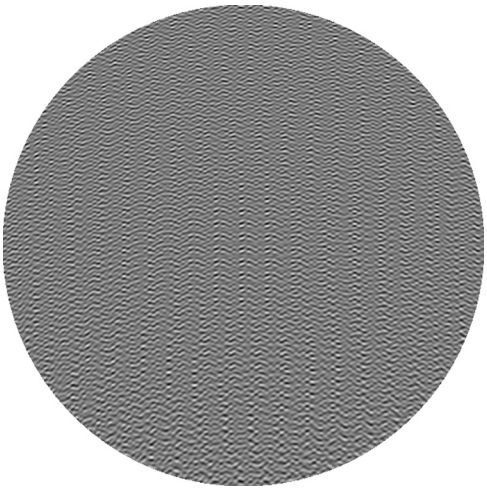

Fig. 3. Computer-generated holograph.

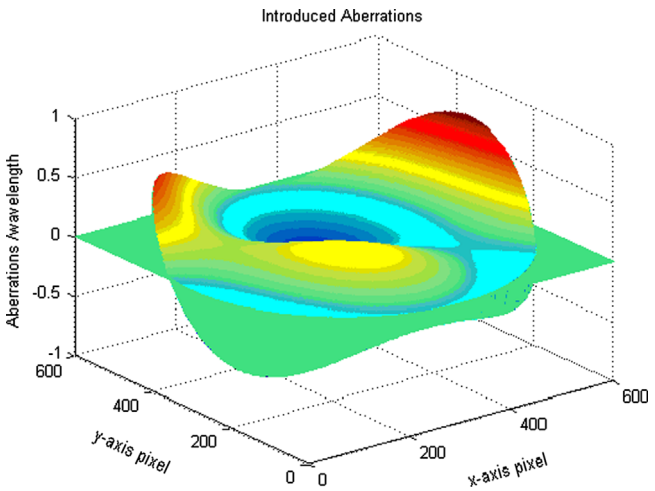

Fig. 4. Distribution of introduced aberrations, RMS = 0.1604λ, PV = 1.2484λ.

where $U_{R,0}$ is the amplitude of the reference laser beam, and $\phi(r_R)$ is the phase function of the reference laser beam.

The two waves interfere in the recording medium, and generate a holographic pattern. If we use a replay laser beam with random aberrations to illuminate the holographic pattern, the wave-front of signal laser beam can be reconstructed on the focal plane. The random aberrations, we mention here, allow for the time-variable laser beam phase distortion, caused by atmosphere turbulence. The diffraction field distribution on the focal plane shall be expressed as

$$U_d(r_d) = \int (U_S^* U_R + c.c) U_P(r_P, r) G(r_d, r)\, dr \tag{5}$$

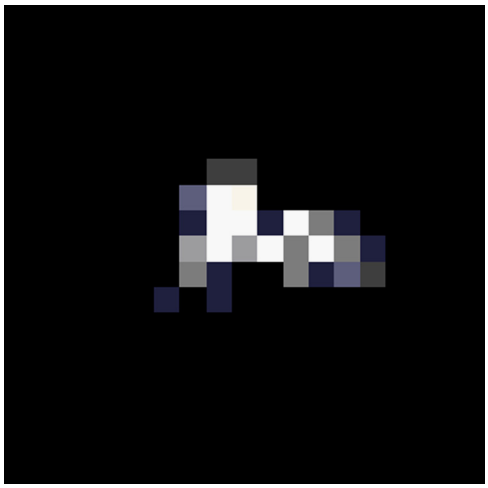

Fig. 5. Intensity distribution on the focal plane before correction (partial enlargement).

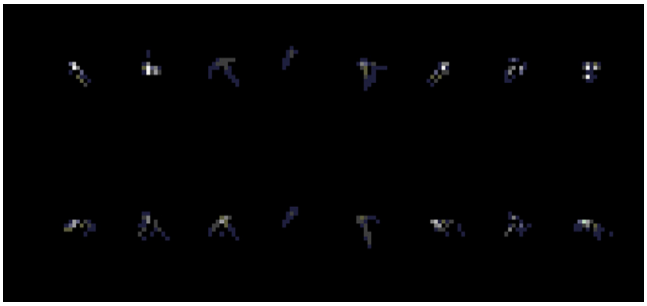

Fig. 6. The distribution of the speckle on a holographic image plane.

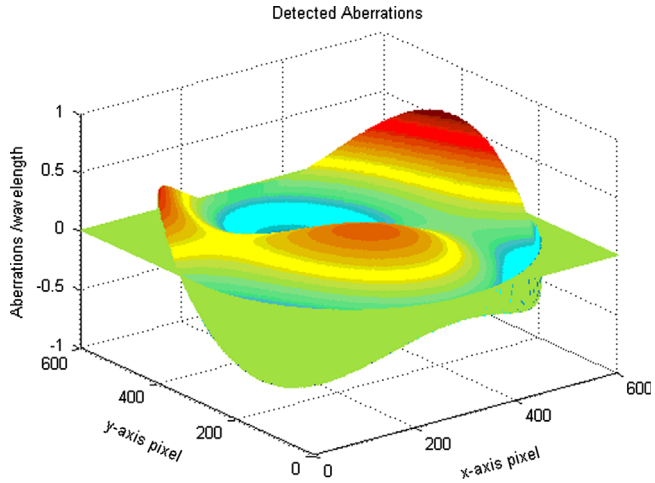

Fig. 7. Distribution of detected aberrations, RMS = 0.1741λ, PV = 1.3134λ.

where $c.c$ is a constant, U_S^* is the conjugate of $U_S(r)$, $U_P(r_P, r)$ is the replay laser beam, and the $G(r_d, r)$ is the Green Function. In free space, $G(r_d, r)$ can be approximately expressed as

$$G(r_d, r) = \frac{\exp\{ik_d[(x_d-x)^2+(y_d-y)^2+(z_d-z)^2]^{1/2}\}}{z_d} \tag{6}$$

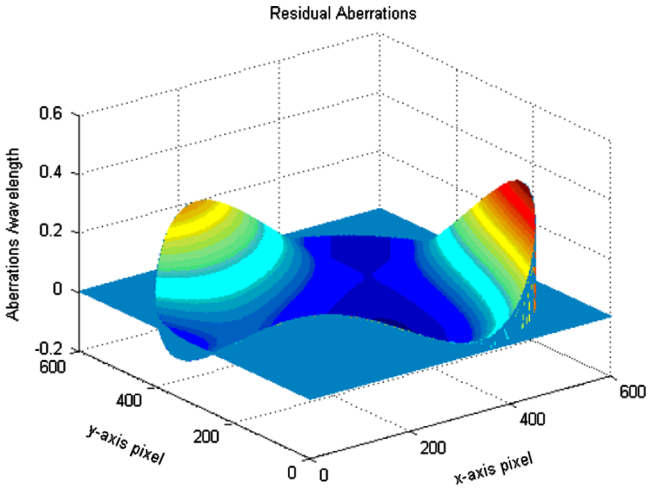

Fig. 8. Distribution of residual aberrations, RMS = 0.0733λ, PV = 0.4498λ.

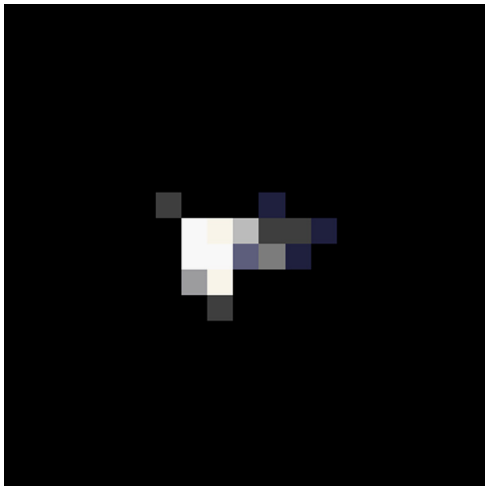

Fig. 9. Intensity distribution on focal plane after correction (partial enlargement).

where k_d is the wave vector of laser beam $U_d(r_d)$ and (x_d, y_d, z_d) and (x, y, z) are space coordinates.

Satisfying Fresnel approximation condition, the secondary phase factor of Eq. (6) can be expanded as

$$[(x_d-x)^2+(y_d-y)^2+(z_d-z)^2]^{1/2} \approx z_d\left[1+\frac{(x_d-x)^2+(y_d-y)^2}{2{z_d}^2}\right]+z\left[1-\frac{(x_d-x)^2+(y_d-y)^2}{2{z_d}^2}\right] \tag{7}$$

Concerning the thickness L of the holograph, the complex amplitude distribution of an image plane is given by

$$\begin{aligned} U_d(r_d) \approx & \int_{-\infty}^{\infty} dV \exp\left[-ik_S z\left(1-\frac{\xi_R}{z_R}\right)\right] \\ & \exp(-ik_S\xi_R)\exp\left[ik_d z\left(1-\frac{\xi_d}{z_d}\right)\right]\exp(ik_d\xi_d) \\ & \times\exp[-iW(x,y)]\prod(x-a,y-b)U_P(r_P) \end{aligned} \tag{8}$$

where $\xi_R = ((x_R-x)^2+(y_R-y)^2/2z_R)$ and $\xi_a = ((x_a-x)^2+(y_a-y)^2/2z_a)$, Π is the pupil function, restricting the integral scope into the pupil, the volume of the holograph is $V = abL$.

Neglecting the thickness of the holograph, Eq. (8) can be further simplified as

$$\begin{aligned} U_d(r_d) \approx & \int_{-\infty}^{\infty} dx \int_{-\infty}^{\infty} dy \exp\left[-i\pi\frac{(x_R-x)^2+(y_R-y)^2}{\lambda z_R}\right] \\ & \times\exp\left[i\pi\frac{(x_d-x)^2+(y_d-y)^2}{\lambda z_d}\right] \\ & \times\exp[-iW(x,y)]\prod(x-a,y-b)U_P(x_P,y_P) \end{aligned} \tag{9}$$

where the range of integration is limited within pupil. a and b are respectively the length and width of the hologram. Processing the secondary phase factor of Eq. (9), we have

$$\begin{aligned} U_d(r_d) \approx & \exp\left(i\pi\frac{{x_d}^2+{y_d}^2}{\lambda z}\right)\iint\exp\left[-i\pi\frac{(x_R-x)^2+(y_R-y)^2}{\lambda z}\right] \\ & \times\exp\left(i\pi\frac{x^2+y^2}{\lambda z}\right)\times\exp[-iW(x,y)]\prod(x-a,y-b)U_P(x_P,y_P) \\ & \times\exp\left(-i2\pi\frac{xx_d+yy_d}{\lambda z}\right)dx\,dy \\ \approx & \exp\left(i\pi\frac{{x_d}^2+{y_d}^2}{\lambda z}\right) \\ & \times F\left\{\exp\left[-i\pi\frac{(x_R-x)^2+(y_R-y)^2}{\lambda z}\right]\exp[-iW(x,y)]\right. \\ & \left.\times\prod(x-a,y-b)U_P(x_P,y_P)\right. \end{aligned}$$

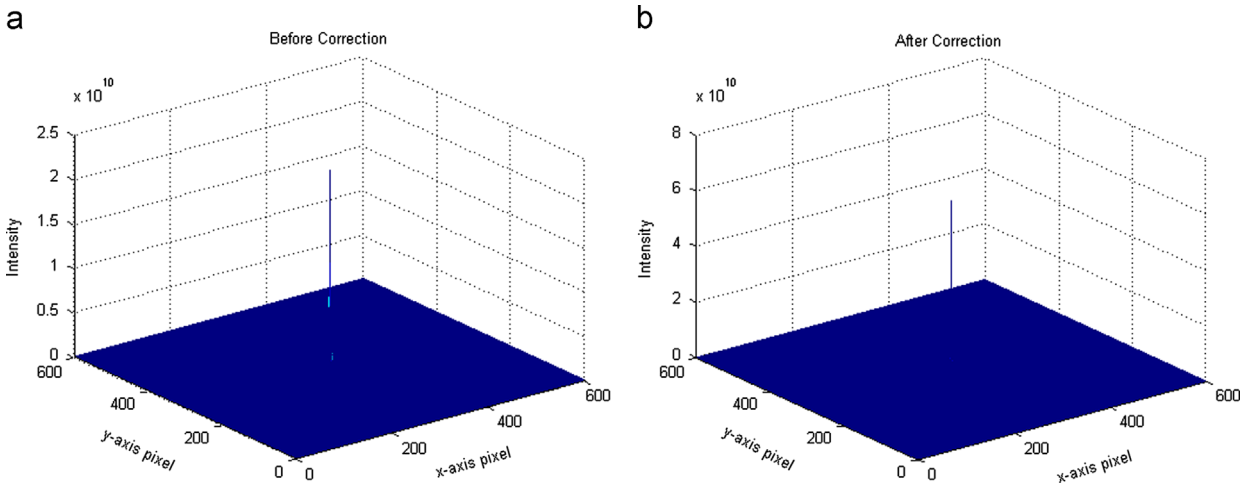

Fig. 10. Comparison of the intensity distribution before and after correction.

$$\exp\left(i\pi\frac{x^2+y^2}{\lambda z}\right)\Big\}_{f_x=(x_d/\lambda z)f_y=(y_d/\lambda z)} \tag{10}$$

where $F\{.\}$ is the Fourier transform.

Based on the above analysis, Fresnel integral, under thin hologram assumption conditions, is simplified into Fourier transform. Thus, it is simple to compute fast Fourier transform (FFT), and then the distribution of complex amplitude on holographic plane can be solved by the numerical method.

2.3. Fiber coupling efficiency analysis of FSO communication system

Generally, the received laser carrier signal should be firstly coupled into a single-mode fiber (SMF) in order to be amplified, detected or de-multiplexed [32,33]. The fiber coupling efficiency of the SMF is defined as the ratio of the average power coupled into the fiber to the average power on the receiver aperture plane [34], which is given by the following equation:

$$J\infty\frac{\left|\iint A_f(r)M_0^*(r)d^2r\right|^2}{\iint A_f(r)A_f{}^*(r)d^2r\times\iint M_0(r)M_0^*(r)d^2r} \tag{11}$$

where $A_f(r)$ is the Fourier transform of the single-mode fiber optical field, $M_0(r)$ is the incident optical field on the focal plane, $A_f(r)$ and $M_0(r)$ are complex quantities. Since Eq. (11) is too complex to calculate, the Strehl ratio is introduced to approximate the average fiber coupling efficiency [35], as given by the following equation:

$$ST\infty|A_f(r_0)|^2 \tag{12}$$

where r_0 is the desired on-axis location of the center of the fiber end within this plane. In this paper, we will calculate the Strehl ratio of the laser images on the focal plane before and after aberrations compensation respectively to analyze the fiber coupling efficiency.

Table 1
Fiber coupling efficiency before and after aberrations correction.

Coupling efficiency before correction	Coupling efficiency after correction
0.2198	0.5993

3. Numerical simulation

In terms of the computer-generated holograph, the center wavelength of the laser is $\lambda = 632.8$ nm, the number of sampling points of

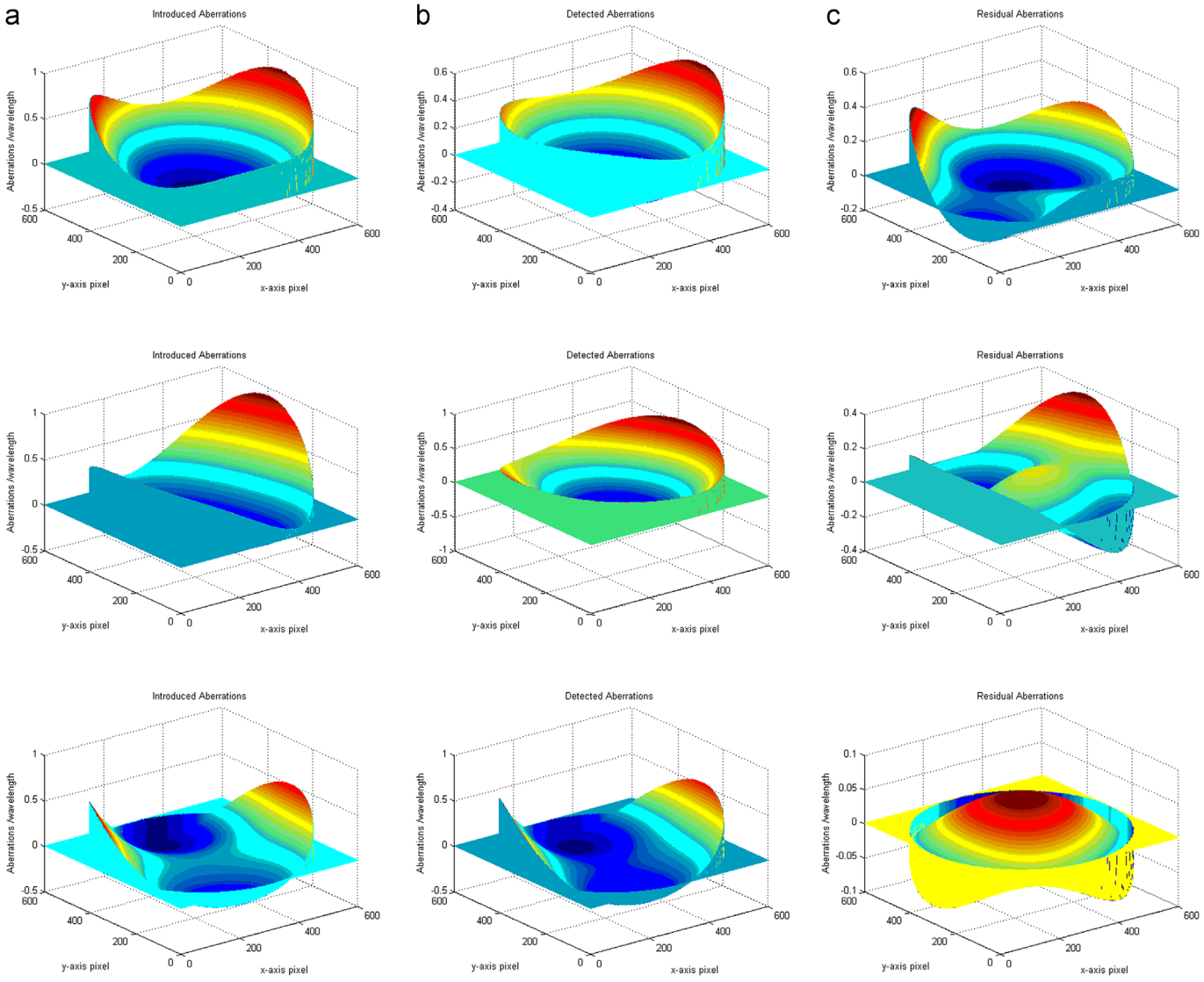

Fig. 11. Results of the six groups simulation.

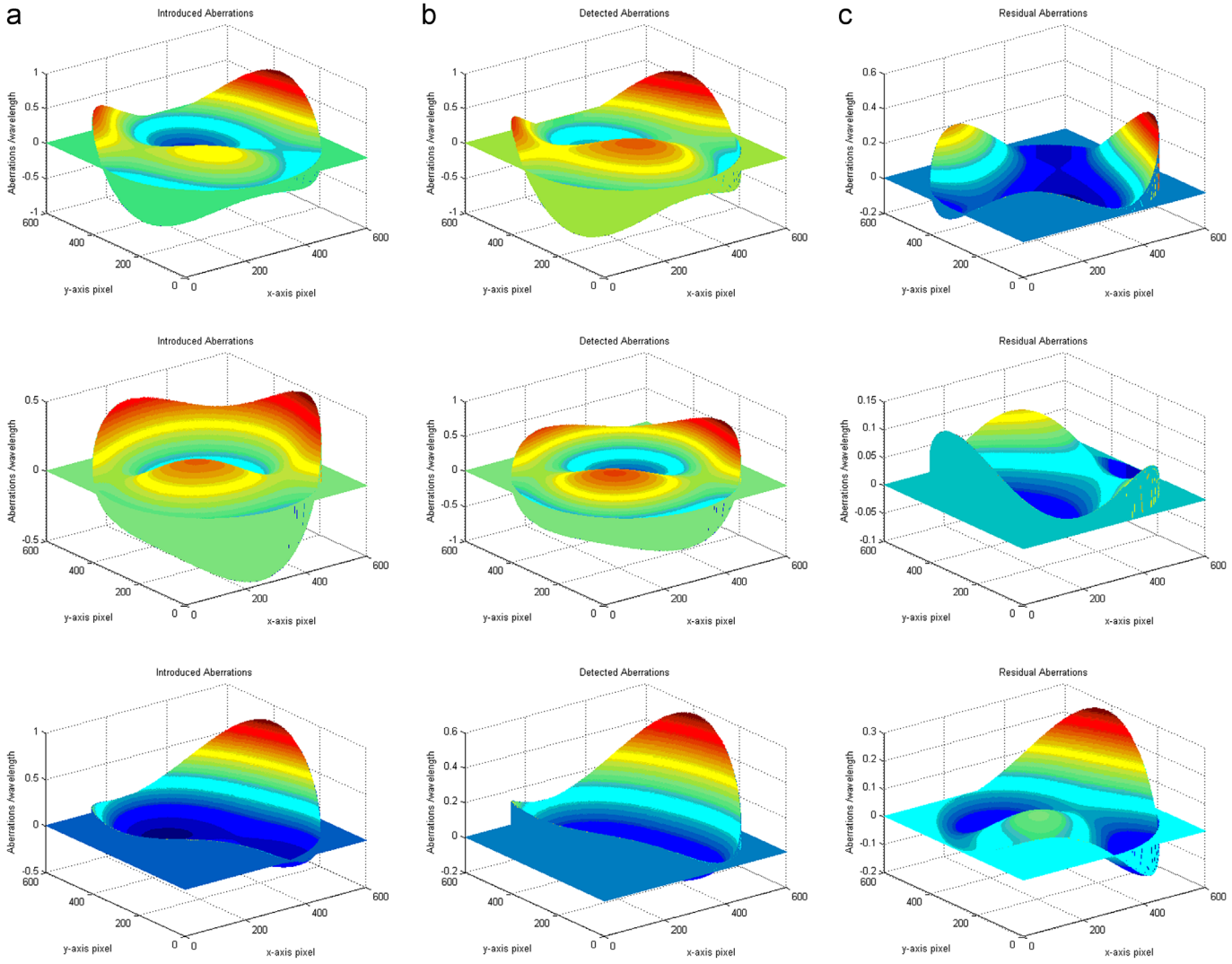

Fig. 11. (*continued*)

holographic grating is 600 × 600 pixels, the aperture of holographs is 60 mm, the distance between the image plane and the holographic plane is 1500 mm, the off-axis distance of the spot on focal plane is larger than 1 cm. We code the low eight order Zernike aberrations (Z3, Z4, …, Z10). Where the peak-to-valley (PV) value of Z3, Z4, Z5 is $\lambda/2$, and the PV value of Z6, Z7, Z8, Z9, Z10 is $\lambda/4$. The holograph we eventually obtained is shown in Fig. 3.

Then, we detect the Zernike aberrations based on the holograph, as shown in Fig. 3. Before detection, the relationship of relative intensity and Zernike item is calibrated. The calibration method is as follows: at first, a certain Zernike aberration is introduced independently, and then the amplitude of this aberration is adjusted continuously. Simultaneously, the relative intensity of the spots within detector aperture is detected on the holographic image plane. By the above calibration method, the sensing response sensitivity of every Zernike aberrations is obtained. Thus, the incoming wave with the low eight orders of Zernike aberration is generated, as shown in Fig. 4.

Where RMS is the value of root-mean-square and PV is the value of peak-to-valley. The intensity distribution on focal plane (detail view) is as shown in Fig. 5.

The intensity distribution of the speckle on the holographic image plane is shown in Fig. 6.

By comparing the relative intensity on the holographic image plane, the values of Zernike aberrations obviously can be determined. Thus, the reconstructed wave-front is shown in Fig. 7. Similarly, the wave-front can be described by the RMS value and the PV value.

In order to analyze the accuracy of wave-front sensor we proposed, we can calculate the residual aberrations between introduced and detected aberrations. The residual aberrations' distribution is shown in Fig. 8.

Thus, it can be seen that the holographic modal wave-front sensor has smaller residual in low eight orders' Zernike aberrations' detection. The intensity distribution on focal plane after aberrations correction is shown in Fig. 9.

Then, we analyze the intensity distribution before and after aberrations correction, as shown in Fig. 10.

Where Fig. 10(a) is the intensity distribution before aberrations correction and Fig. 10(b) is the intensity distribution after aberrations correction. In this paper, the Strehl ratio is calculated as

$$ST = \frac{|\mathrm{MAX}\,[A(i)]|^2}{\left|\sum_{i=1}^{N}[A(i)^2]\right|} \tag{13}$$

where $A(i)$ is the gray value of the ith pixel, and N is the number of pixels. According to Eq. (13), we analyze the fiber coupling efficiency before and after aberrations' correction. The results are shown in Table 1.

Table 2
Statistical property of simulation results.

No.	Introduced aberrations RMS (λ)	Detected aberrations RMS (λ)	Introduced aberrations PV (λ)	Detected aberrations PV (λ)	Residual aberrations RMS (λ)	Residual aberrations PV (λ)	Coupling efficiency before correction	Coupling efficiency after correction
1	0.2232	0.1602	1.2539	0.8024	0.0821	0.5610	0.0971	0.5678
2	0.2460	0.1653	1.2994	0.8227	0.1095	0.6772	0.0819	0.4424
3	0.1463	0.1565	0.8863	0.9143	0.0267	0.1250	0.2972	0.7549
4	0.1604	0.1741	1.2484	1.3134	0.0733	0.4498	0.2198	0.5993
5	0.1383	0.1523	0.9443	1.0245	0.0338	0.2141	0.2906	0.7390
6	0.1623	0.1266	1.0896	0.7469	0.0548	0.4240	0.2836	0.6751

In this paper, we make six groups numerical simulation by changing the introduced aberrations. In the same way, we get the six group results mainly including wave-front distribution of the introduced, detected and residual aberrations as shown in Fig. 11. Where Fig. 11(a) shows the introduced aberrations, Fig. 11 (b) shows the detected aberrations, and Fig. 11(c) shows the residual aberrations. The statistical properties, mainly including RMS value, PV value and the fiber coupling efficiency before and after aberrations correction, are shown in Table 2.

As shown in Table 2, we can see that it fits for weak atmospheric turbulence when the RMS value of the aberration is less than 1.15λ and the PV value less than 1.0λ. Under this condition, the RMS value of the residual aberrations is less than 0.04λ and the PV value less than 0.25λ. The fiber coupling efficiency increases from nearly 30% to more than 70%. However, the RMS value of residual aberrations is more than 0.07λ with stronger atmospheric turbulence, when the RMS value of introduced aberrations is more than 0.2λ and the PV value is more than 1.2λ. Under this condition, the fiber coupling efficiency is only less than 10%. It increases to around 50% after aberrations correction. Above all, the wave-front sensor we proposed is better for weak atmospheric turbulence.

4. Conclusion

In this paper, we propose a new wave-front aberration measurement method which uses HMWFS in AO system for FSO communication system. We analyzed the principle of HMWFS in theory and simulated the procedure of wave-front aberrations detection based on HMWFS. And then we discussed the impact of HMWFS on fiber coupling efficiency of the FSO communication system before and after the aberrations correction. According to the results of numerical simulation, HMWFS is better for weak atmospheric turbulence while fast detecting rates and insensitivity to beam scintillation are its biggest advantage in the FSO communication system.

The disturbance strength is only described by the RMS value and PV value of the wave-front distribution in our work. Further work about the relationship between the introduced aberrations and the structure constant of refractive index C_n^2 will be carried out in the near future. In addition, an experimental system of wave-front sensing based on HMWFS will be setup in the future work.

Acknowledgment

This work was supported by the National Natural Science Foundation of China (Nos. 60972028 and 61373124).

References

[1] Willebrand H, Ghuman BS. Free space optics: enabling optical connectivity in today's networks. Indianapolis, IN: Sams; .
[2] van Eekeren Adam WM, Schutte Klamer, Dijk Judith. Turbulence compensation: an overview. Proc. SPIE 2012;8355 (83550Q-1–83550Q-10).
[3] Sheng Ming, Xie Xiu-xiu. Average bit error rate analysis for free-space optical communications over weak turbulence with pointing errors. Opt Eng 2012;51 (10)105009-1–90-5.
[4] Anguita Jaime A, Neifeld Mark A, Hildner Björn, Rateless Bane Vasic. Coding on experimental temporally correlated FSO channels. J Lightwave Technol 2010;28(7):990–1002.
[5] Kevin Murphy, Daniel Burke, Chris Dainty Nicholas Devaney. Experimental detection of optical vortices with a Shack–Hartmann wave-front sensor. Opt Exp 2010;18(15):15448–60.
[6] Yuhui Chen Lu, Huang Lin, Gan Zhiyuan Li. Wave-front shaping of infrared light through a subwavelength hole. Light: Sci Appl 2012.
[7] Stassinakis AN, Nistazakis HE, Peppas KP, Tombras GS. Improving the availability of terrestrial FSO links over log normal atmospheric turbulence channels using dispersive chirped Gaussian pulses. Opt Laser Technol 2013;54 (30 December):329–34.
[8] Xiang Yi Zengji Liu, Peng Yue. Optical scintillations and fade statistics for FSO communications through moderate-to-strong non-Kolmogorov turbulence. Opt Laser Technol 2013;47(April):199–207.
[9] Nahar Niro K, Rojas Roberto G. Efficient free-space coupling to LMA-PCF by aberration correction. IEEE Trans Compon Packaging Manufact Technol 2011;1 (October (10)).
[10] Dikmelik Yamaç, Davidson Frederic M. Fiber-coupling efficiency for free-space optical communication through atmospheric turbulence. Appl Opt 2005;44(10 August (23)):4946–52.
[11] Ma Jing, Zhao Fang, Tan Liying, Yu Siyuan, Yang Yuqiang. Degradation of single-mode fiber coupling efficiency due to localized wave-front aberrations in free-space laser communications. Opt Eng 2010;4(April (045004)):1–649 2010;4(April (045004)):1–6.
[12] Toyoshima Morio. Maximum fiber coupling efficiency and optimum beam size in the presence of random angular jitter for free-space laser systems and their applications. J Opt Soc Am A 2006;23(September (9)):2246–50.
[13] Liu Wei, Shi Wenxiao, Wang Bin, Yao Kainan, Lv Yaowen, Wang Jihong. Free space optical communication performance analysis with focal plane based wave-front measurement. Opt Commun 2013;309:212–20.
[14] Zepp A. Holographic wavefront sensing with spatial light modulator in context of horizontal light propagation. SPIE; 2012 (8535), Bellingham USA.
[15] Tyson RK. Principles of adaptive optics. 2nd ed.. Boston, MA: Academic; 1998.
[16] Tenghao Li Mali, Gong Lei, Huang Yuntao, Qiu Qiao Xue. Weighted fried reconstructor and spatial-frequency response optimization of Shack–Hartmann wave-front sensing. Appl Opt 2012;5(29):7115–23.
[17] Liu Wei, Shi Wenxiao, Cao Jingtai, Lv Yaowen, Yao Kainan, Wang Shuai, et al. Bit error rate analysis with real-time pointing errors correction in free space optical communication systems. Optik 2013.
[18] Lin V, Wei H-C, Hsieh H-T, Hsieh J-L, Su G-DJ. Design and fabrication of long-focal-length microlens arrays for Shack–Hartmann wave-front sensors. Micro Nano Lett 2011;6(7):523–6.
[19] Jiang Minshan, Zhang Xiangyang, Puliafito Carmen A, Zhang Hao F, Jiao Shuliang. Adaptive optics photoacoustic microscopy. Opt Exp 2010;18(21):21770–6.
[20] Weyrauch, Thomas, Vorontsov, Mikhail A. Atmospheric compensation with a speckle beacon in strong scintillation conditions: directed energy and laser communication applications. Appl Opt 2005;44(30):6388–401.
[21] Liqiang Han, Katsunori Shida, Qi Wang, Zhiquan Li. Free space optical communication system based on wave-front sensorless adaptive optics. Proc SPIE 2009;7513 (75130X:1-4).
[22] Zheng Yi, Wang Xiaohua, Deng Li, Shen Feng, Li Xinyang. Experimental investigation of segmented adaptive optics for spatial laser array in an atmospheric turbulence condition. Opt Commun 2011;284:4975–82.
[23] Song H, Fraanje R, Schitter G, Kroese H, Vdovin G, Verhaegen M. Model-based aberration correction in a closed-loop wave-front -sensor-less adaptive optics system. Opt Exp 2010;18(23):24070–84.
[24] Kruschwitz BE, Bahk S-W, bromage J, Moore MD, Irwin D. Accurate target-plane focal-spot characterization in high-energy laser systems using phase retrieval. Opt Exp 2012;20(19)20874–83.
[25] Xue Bindang, Zheng Shiling. Phase retrieval using the transport of intensity equation solved by the FMG-CG method. Optik 2011;122:2101–6.

[26] Mishra Sanjay K, Bhatt Rahul, Mohan Devendra, Arun Kumar Gupta, Anurag Sharma. Differential modal Zernike wave-front sensor employing a computer-generated hologram: a proposal. Appl Opt 2009;48(20 November (33)):6458–65.
[27] Thomas CE, Baylor LR, Combs SK, Meitner SJ, Rasmussen DA, Granstedt EM, et al. High speed digital holography for density and fluctuation measurements. Rev Sci Instr 2010;81:1–7 (10E527).
[28] Shabanov DV, Geliknovand GV, Gelikonov VM. Broadband digital holographic technique of optical coherence tomography for 3-dimensional biotissue visualization. Laser Phys Lett 2009;6:753.
[29] Čižmár T, Brzobohatý O, Dholakia K, Zemánek P. The holographic optical micro-manipulation system based on counter-propagating beams. Laser Phys Lett 2011;8:50.
[30] Chirita A, Kukhtarev N, Korshak O, Prilepov V, Jidcov Iu. Recording holograms of micro-scale objects in real time. Laser Phys Lett 2013;23:036002.
[31] Andersen Geoff, Ghebremichael Fassil, Baker Jeff, Gaddipati Ravi, Gaddipati Phani. Holographic adaptive laser optics system. SPIE; 2012; 1–8, Bellingham USA.
[32] Dussan Luis, Ghebremichael Fassil, Kenny Chen. Holographic wave-front sensor. Opt Eng 2009;48(August (8)):1–5(085801).
[33] Zhao Xin, Jiang Huilin, Han Chen. Fiber coupling efficiency on focal plane spot extension caused by turbulence. Optik 2013;124(June (12)):1113–5.
[34] Wu Hanling, Yan Haixing, Li Xinyang. Modal correction for fiber-coupling efficiency in free-space optical communication systems through atmospheric turbulence. Optik 2010;121(October (19)):1789–93.
[35] Weyrauch Thomas, Vorontsov Mikhail A, Gowens II John W, Bifano Thomas G. Fiber coupling with adaptive optics for free-space optical communication. SPIE; 2002; 117–84, Bellingham USA.